Vietnam Journal of Catalysis and Adsorption
Tạp chí xúc tác và hấp phụ Việt Nam

https://jca.edu.vn

Synthesis of rGO/PANi/MnO_2 ternary nanocomposite used for supercapacitor electrode by 3D printing and electrodeposition techniques

Do Thi Thuy[1,*], Nguyen Tuan Dung[2], Le Trong Lu[2], Nguyen Le Huy[3]

[1] *Institute of Materials, Biology and Environment, Academy of Military Science and Technology, 17 Hoang Sam road, Hanoi, Vietnam.*
[2] *Institute of Materials Science, Vietnam Academy of Science and Technology, 18 Hoang Quoc Viet road, Hanoi, Vietnam*
[3] *School of Chemistry and Life Sciences, Hanoi University of Science and Technology, 1 Dai Co Viet road, Hanoi, Vietnam*
** Email: dothuyvlnn@gmail.com*

ARTICLE INFO

Received: 05/09/2025
Accepted: 23/09/2025
Published: 30/09/2025

Keywords:
3D printing;
electrochemical supercapacitor;
reduced graphene oxide;
polyaniline;
manganese dioxide.

ABSTRACT

Three-dimensional (3D) printing has emerged as a promising method for fabricating advanced electrode materials. In this study, a ternary nanocomposite film of reduced graphene oxide (rGO), polyaniline (PANi), and MnO_2 nanoparticles was prepared by 3D printing and electrochemical deposition for high-performance supercapacitors. A printable GO/aniline ink (1:1 mass ratio) was printed and electrochemically treated in 0.1 M H_2SO_4: first reduced at –0.8 V for 30 s, then electropolymerized by cyclic voltammetry (–0.4 to +0.95 V). MnO_2 was subsequently electrodeposited at +0.6 V for 200 s in $MnSO_4/H_2SO_4/KCl$ solution. FE-SEM/EDX confirmed uniform MnO_2 distribution (~2 wt%). Electrochemical tests in 1 M H_2SO_4 showed enhanced capacitance and stability, with the rGO/PANi/MnO_2 electrode reaching 740 F/g at 1 A/g and retaining 97% capacitance after 5000 cycles at 15 A/g.

Introduction

Supercapacitors have attracted extensive attention as energy storage devices due to their outstanding charge-discharge capability and high-power density. However, their relatively low energy density (typically 5–80 Wh/kg) requires larger component sizes than conventional batteries, significantly limiting their broad practical application [1]. According to their energy storage mechanisms, supercapacitors can be classified into two categories: electric double-layer capacitors (EDLCs) and pseudocapacitors (PCs). EDLCs generally employ carbon-based materials due to their large surface area and superior electrical conductivity [2,3]. Since its discovery in 2004, graphene has received considerable interest as an electrode material for supercapacitors, attributed to its exceptional conductivity and ultrahigh specific surface area [4]. Although graphene exhibits significantly higher capacitance than other carbon materials, theoretical predictions indicate that under ideal conditions (monolayer graphene with complete surface utilization), the maximum achievable capacitance is limited to approximately 550 F g^{-1} [5]. Hybridizing graphene with pseudocapacitive materials, particularly conducting polymers such as polyaniline (PANi) and polypyrrole, has been extensively explored to overcome this limitation. Consequently, graphene/conducting polymer hybrids are promising candidates for high-capacitance and stable supercapacitor electrodes [6–9]. Notably, ternary hybrid systems such as rGO/PANi/MnO_2 have gained considerable attention because they combine the high conductivity of rGO, the pseudocapacitance of PANi,

https://doi.org/10.62239/jca.2025.046

and the high theoretical capacitance of MnO_2. This synergistic integration enhances energy storage capability while improving cycling durability, positioning rGO/PANi/MnO_2 composites as one of the most promising platforms for next-generation supercapacitors.

Given the poor dispersibility of pristine graphene in conventional solvents, graphene oxide (GO) is frequently employed as a precursor. However, its intrinsically low electrical conductivity requires chemical or electrochemical reduction to produce reduced graphene oxide (rGO). In a recent work, Moussa et al. [9] fabricated GO/PANi composite films and achieved a specific capacitance of 513.5 F g^{-1} at 10 wt% PANi loading. Further performance enhancement can be achieved by incorporating transition metal oxide nanoparticles into rGO/conducting polymer systems. For instance, Tang et al. reported a ternary PANi/GO/MnO_2 nanocomposite film, in which the incorporation of MnO_2 nanorods significantly improved the electrochemical performance, forming a specific capacitance of 512 F g^{-1} with excellent cycling stability [10].

Simultaneously, three-dimensional (3D) printing technology has recently emerged as an innovative manufacturing platform with broad applications across diverse fields. In electronic device fabrication, 3D printing enables rapid, precise, and customizable electrode architectures [11,12]. Based on these advances, the present study reports the fabrication and characterization of a ternary rGO/PANi/MnO_2 nanocomposite film using a combined strategy of 3D printing and electrochemical deposition. The structural, morphological, and electrochemical properties of the resulting composite electrodes were systematically investigated to develop high-performance supercapacitor devices.

Experimental

Chemical

All chemicals used in this study were of analytical grade and purchased from suppliers in China, including graphite powder, graphite substrate, aniline, MnSO4 · 2H2O, KCl, $KMnO_4$, and the acids H_2SO_4, H_3PO_4, and HNO_3.

Fabrication of rGO/PANi composite film modified with MnO_2 nanoparticles

Preparation of rGO/PANi film

A GO/aniline (GO/ANi) ink was prepared and employed for 3D printing composite films. Graphene oxide (GO) was synthesized by a modified Tour method [13]. In a typical procedure, 0.2 g of GO was dispersed in 20 mL of deionized water, followed by the addition of aniline monomer at different mass ratios of GO:ANi = 2:1, 1:1, and 1:2. The resulting suspension was ultrasonicated for 1 h to obtain a homogeneous and stable GO/ANi ink (with a viscosity of 20÷30 mPa.s, measured at room temperature). Nanocomposite films were fabricated using a home-made 3D printer developed at the Vietnam Academy of Science and Technology. Printing was performed under SolidWorks control with the following parameters: printing speed of 2 mm/s, layer thickness of 0.2 mm, line width of 0.25 mm, and bed temperature of 80 °C. The films (2.0 × 1.0 cm^2) were printed directly onto graphite substrates.

Since both GO and aniline are intrinsically non-conductive, the printed films were subjected to a two-step electrochemical treatment in 0.1 M H_2SO_4: (i) electrochemical reduction of GO to rGO at a constant potential of –0.8 V vs. SCE for 10–40 s, and (ii) electropolymerization of aniline by cyclic voltammetry within the potential range of –0.4 to +0.95 V at a scan rate of 50 mV s^{-1} [14]. Electrochemical processes were conducted on a Biologic VSP 300 workstation in a conventional three-electrode configuration, employing the nanocomposite film as the working electrode (WE), a saturated calomel electrode (SCE) as the reference, and a Pt mesh as the counter electrode. The obtained rGO/PANi films were rinsed thoroughly with deionized water and ethanol and dried under ambient conditions before further characterization.

Electrodeposition of MnO_2 onto rGO/PANi film

MnO_2 nanoparticles were electrochemically deposited onto the rGO/PANi surface following established procedures [15,16]. The deposition was carried out in a mixed electrolyte containing 0.2 M H_2SO_4, 0.5 M KCl, and 50 mM $MnSO_4$ under a constant potential of +0.6 V vs. SCE. Deposition times of 100, 200, and 300 s were systematically investigated. The as-prepared rGO/PANi/MnO_2 films were rinsed with deionized water and dried before characterization.

Characterization of rGO/PANi/MnO_2 nanocomposite electrodes

The morphological features and elemental composition of the nanocomposite films were examined by field-emission scanning electron microscopy (FE-SEM, Hitachi S4800) coupled with energy-dispersive X-ray spectroscopy (EDX). Electrochemical behavior was evaluated by cyclic voltammetry (CV), while capacitive performance was assessed by galvanostatic charge–

https://doi.org/10.62239/jca.2025.045

discharge (GCD) measurements. The specific capacitance (C_s, F g^{-1}) was determined according to the following equation:

$$C_s = \frac{I.\Delta t}{m.\Delta V}$$

Where I is the discharge current (A), Δt is the discharge time (s), ΔV is the potential window (V), and m is the mass of the active material (g).

Results and discussion

Synthesis of rGO/PANi nanocomposite films modified with MnO_2

A printable GO/ANi ink with a mass ratio of 1:1 was used to fabricate GO/ANi films by 3D printing. The printed electrodes were subsequently subjected to a two-step electrochemical treatment in 0.1 M H_2SO_4: (i) electrochemical reduction of GO to rGO at –0.8 V vs. SCE, and (ii) electropolymerization of aniline through cyclic voltammetry (CV) within the potential range of –0.4 to +0.95 V. The corresponding results are presented in Figure 1.

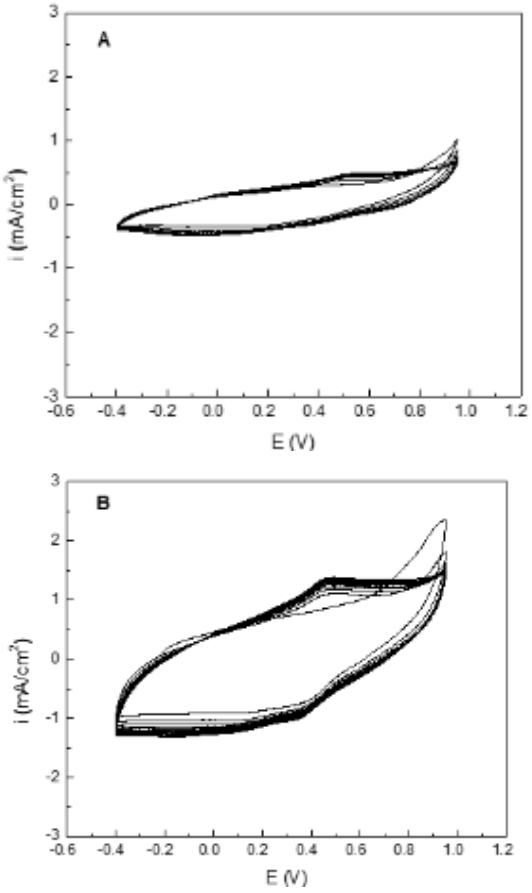

Figure 1: CV curves recorded on GO/ANi printed electrodes in 0.1 M H_2SO_4: (A) without GO reduction, (B) after 30 s of GO reduction

Figure 1 displays the CV curves obtained from GO/ANi-printed electrodes in 0.1 M H_2SO_4. In the absence of GO reduction, only very low current responses were observed (Figure 1A). By contrast, the reduced sample exhibited a clear beginning of aniline oxidation at +0.62 V during the first cycle, followed by a progressive increase in redox peak currents in the following scans (Figure 1B). These results confirm the successful electropolymerization of PANi within the 3D-printed GO/ANi films and underscore the essential role of GO reduction at –0.8 V in enhancing electrical conductivity and facilitating efficient PANi growth.

Effect of GO reduction time and ANi content

The effect of GO reduction time was investigated within the range of 10–40 s. The resulting rGO/PANi films were evaluated by cyclic voltammetry (CV) in 1 M H_2SO_4 from –0.2 to +0.8 V, which was selected to maintain the electrochemical stability of PANi (Figure 2A).

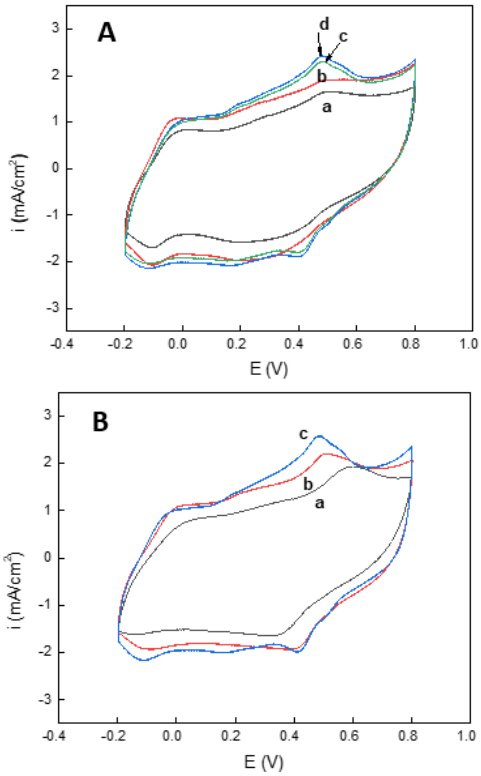

Figure 2: CV curves of rGO/PANi electrodes synthesized with different: (A) GO reduction times: (a) 10 s, (b) 20 s, (c) 30 s, (d) 40 s and (B) GO: ANi ratios in 1 M H_2SO_4: (a) 2:1, (b) 1:1, (c) 1:2.

The CV curves in Figure 2A exhibit the characteristic redox peaks of PANi at –0.02/–0.12 V and +0.48/+0.41 V [17]. Electrochemical activity progressively increased with longer reduction times, reaching its maximum at

40 s. Nevertheless, the improvement beyond 30 s was minimal, and prolonged reduction at –0.8 V introduced the risk of film debonding. Accordingly, a reduction time of 30 s was identified as the optimal condition and was adopted for subsequent experiments. This condition ensured a balance between high electrochemical activity and mechanical stability of the electrode film, therefore providing reliable performance for further electrochemical evaluation. The CV results in Figure 2B clearly highlight the crucial role of PANi in controlling the electrochemical response of the nanocomposite electrodes. With increasing aniline content, the redox current intensity was significantly enhanced, indicating the contribution of PANi chains in providing abundant redox-active sites and facilitating charge transfer at the electrode–electrolyte interface. However, excessive incorporation of PANi reduced the electrochemical stability of the electrodes and caused undesirable aggregation within the GO/ANi ink. Accordingly, a GO: ANi ratio of 1:1 was determined as the most suitable composition and was adopted for further investigations. This optimized ratio provides a balanced synergy between the conductive rGO framework and the pseudocapacitive PANi phase, ensuring high electrochemical activity and structural stability.

Optimization of MnO_2 deposition time

MnO_2 nanoparticles were deposited onto rGO/PANi films by applying a constant potential of +0.6 V in 50 mM $MnSO_4$ with 0.2 M H_2SO_4 and 0.5 M KCl. Electrodes obtained at different deposition times were evaluated in 1 M H_2SO_4, and the CV curves are shown in Figure 3.

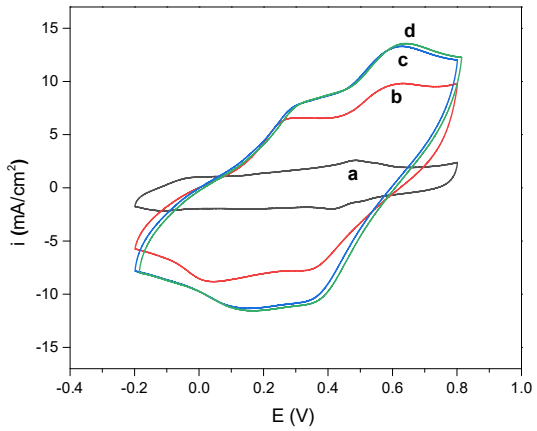

Figure 3: CV curves of (a) rGO/PANi and rGO/PANi/MnO_2 electrodes with deposition times of (b) 100 s, (c) 200 s, and (d) 300 s in 1 M H_2SO_4.

The CV data demonstrate that MnO_2 incorporation significantly enhances redox activity due to its pseudocapacitive contribution [10]. Longer deposition time further increased the current response; however, the improvement from 200 s to 300 s was minimal. Therefore, a deposition time of 200 s was identified as the optimal condition for subsequent experiments. This optimization balances electrode stability and pseudocapacitive performance, providing a reliable foundation for further electrochemical investigations.

Characterization of rGO/PANi/MnO_2 films

FE-SEM analysis

The surface morphology of rGO/PANi films before and after MnO_2 deposition is depicted in Figure 4 (A, B). The FE-SEM images reveal the successful formation of MnO_2 crystallites uniformly distributed across the film surface, indicating effective electrodeposition

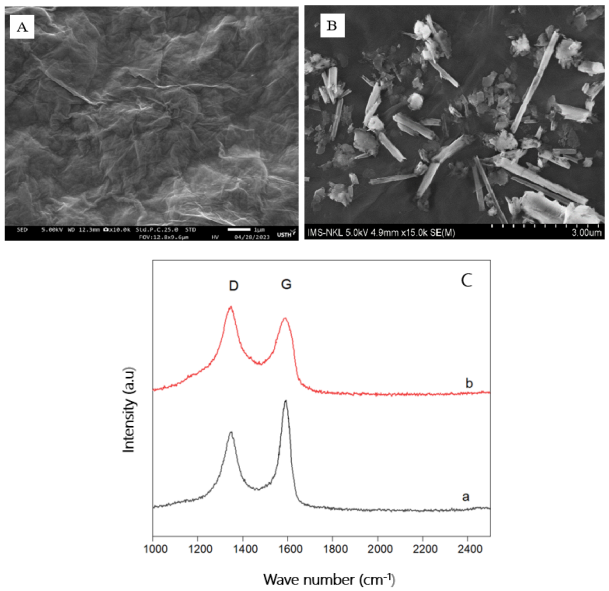

Figure 4: FE-SEM images of (A) rGO/PANi and (B) rGO/PANi/MnO_2 films, (C) Raman spectra of (a) GO/ANi and (b) rGO/PANi/MnO_2

Raman spectra

The structure of the rGO/PANi/MnO_2 composite film was analyzed by Raman spectroscopy, with the GO/ANi sample examined similarly as a reference. The results are presented in Figure 4C. As shown in Figure 4C, characteristic peaks of graphene were observed, including the D band at 1344 cm^{-1} and the G band at 1588 cm^{-1}. The intensity ratio of the D and G bands (I_D/I_G) was 0.86 for GO/ANi (curve a) and increased to 1.20 for rGO/PANi/MnO_2 (curve b), confirming the reduction of GO to rGO.

https://doi.org/10.62239/jca.2025.045

EDX analysis

Table 1: Elemental composition of the rGO/PANi/MnO_2

Element	Atomic (%)	Weight (%)
C	73.01	79.78
O	23.18	19.02
S	1.72	0.70
Mn	2.09	0.50
Total	100	100

Elemental composition of the rGO/PANi/MnO_2 nanocomposite was determined by EDX, and the results are summarized in Table 1. The analysis indicates that the film consists primarily of C (73.01%) and O (23.18%), with minor S (1.72%) originating from the H_2SO_4 electrolyte. Mn was detected at 2.09%, confirming the successful deposition of MnO_2. The incorporation of Mn within the composite matrix demonstrates the effective integration of the metal oxide phase into the conductive rGO/PANi framework, which is essential for enhancing the pseudocapacitive contribution.

Electrochemical capacitive properties

The capacitive properties of rGO/PANi and rGO/PANi/MnO_2 films were investigated in 1 M H_2SO_4 using galvanostatic charge–discharge (GCD) measurements across a current density range of 1–10 A g^{-1} (Figure 5).

Both electrodes exhibited a hybrid charge storage mechanism combining electric double-layer capacitance and pseudocapacitance. The specific capacitance (C_s) gradually decreased with increasing current density, which is typically attributed to the limited ion diffusion and reduced utilization of active sites under high-rate conditions. Significantly, the ternary rGO/PANi/MnO_2 electrode consistently exceeded the binary rGO/PANi electrode across all current densities. At 1 A g^{-1}, the rGO/PANi/MnO_2 electrode obtains a high C_s of 740 F g^{-1}, substantially exceeding previously reported values of ~400 F g^{-1} [14] and 467 F g^{-1} [18]. This enhancement can be explained by the synergistic effect between MnO_2 and PANi: MnO_2 provides additional pseudocapacitive redox sites, while rGO offers a conductive framework that facilitates rapid electron transport and efficient charge transfer at the electrode–electrolyte interface.

Cycling stability was further evaluated at 15 A g^{-1} over 5000 consecutive GCD cycles (Figure 5D). The ternary rGO/PANi/MnO_2 electrode maintained 97% of its initial capacitance, compared to 85% for rGO/PANi. These results demonstrate a cycling durability higher than that reported in related works in the literature. The superior cycling durability can be attributed to the structural reinforcement provided by MnO_2 nanoparticles, which stabilize the volumetric expansion and reduction of PANi during repeated redox cycling. These results confirm that MnO_2 not only enhances capacitance but also significantly improves the long-term reliability of the composite electrode.

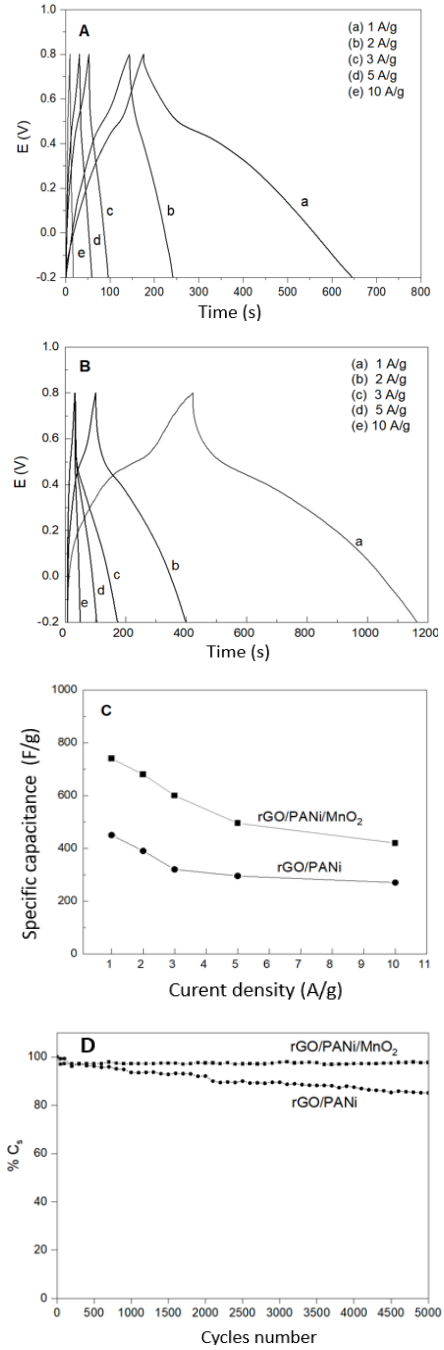

Figure 5: (A) GCD curves of rGO/PANi and (B) rGO/PANi/MnO_2; (C) variation of specific capacitance with current density; (D) capacitance retention of rGO/PANi and rGO/PANi/MnO_2 electrodes after 5000 cycles at 15 A/g

https://doi.org/10.62239/jca.2025.046

Conclusion

A ternary nanocomposite film of reduced graphene oxide (rGO), polyaniline (PANi), and MnO_2 nanoparticles was successfully fabricated by combining 3D printing and electrochemical deposition. Cyclic voltammetry (CV) analysis identified the optimal electrochemical activity for films prepared with a GO: ANi ratio of 1:1, reduced at –0.8 V for 30 s, and electropolymerized in 0.1 M H_2SO_4. Subsequent electrodeposition of MnO_2 at +0.6 V for 200 s produced uniformly distributed nanoparticles, as confirmed by FE-SEM and EDX analysis (~2 wt%). Electrochemical evaluation demonstrated outstanding capacitive behavior, with the rGO/PANi/MnO_2 electrode obtaining a high specific capacitance of 740 F g^{-1} at 1 A g^{-1} and retaining 97% of its capacitance after 5000 cycles at 15 A g^{-1}. In conclusion, these results underscore the potential of 3D-printed rGO/PANi/MnO_2 composites as robust, high-performance, and stable electrode materials for next-generation supercapacitors, while also pointing to opportunities for further optimization and demonstrating strong prospects for commercial application

References

1. D.P. Dubal, O. Ayyad, V. Ruiz, P. Gomez-Romero, Chem. Soc. Rev. 44 (2015) 1777–1790. https://doi.org/10.1039/C4CS00266K
2. L.L. Zhang, X.S. Zhao, Chem. Soc. Rev. 38 (2009) 2520–2531. https://doi.org/10.1039/B813846J
3. J. Liu, J. Wang, C. Xu, H. Jiang, C. Li, L. Zhang, J. Lin, Z.X. Shen, Adv. Sci. 5 (2018) 1700322. https://doi.org/10.1002/advs.201700322
4. C. Soldano, A. Mahmood, E. Dujardin, Carbon 48 (2010) 2127–2150. https://doi.org/10.1016/j.carbon.2010.01.058
5. J. Xia, F. Chen, J. Li, N. Tao, Nat. Nanotechnol. 4 (2009) 505–509. https://doi.org/10.1038/nnano.2009.177
6. H. Gómez, M.K. Ram, F. Alvi, P. Villalba, E. Stefanakos, A. Kumar, J. Power Sources 196 (2011) 4102–4108. https://doi.org/10.1016/j.jpowsour.2010.11.002
7. S. Gupta, C. Price, Compos. B Eng. 15 (2016) 46–59. https://doi.org/10.1016/j.compositesb.2016.08.035
8. F. Shen, D. Pankratov, Q. Chi, Curr. Opin. Electrochem. 4 (2017) 133–144. https://doi.org/10.1016/j.coelec.2017.10.023
9. M. Moussa, M.F. El-Kady, S. Abdel-Azeim, R.B. Kaner, P. Majewski, J. Ma, Compos. Sci. Technol. 160 (2018) 50–59. https://doi.org/10.1016/j.compscitech.2018.02.033
10. G. Han, Y. Liu, L. Zhang, E. Kan, S. Zhang, J. Tang, W. Tang, Sci. Rep. 4 (2014) 4824. https://doi.org/10.1038/srep04824
11. F. Zhou, S. Han, Q. Qian, Y. Zhu, Chem. Phys. Lett. 728 (2019) 6–13. https://doi.org/10.1016/j.cplett.2019.04.062
12. D.T. Tung, L.T.T. Tam, H.T. Dung, N.T. Dung, H.T. Ha, N.T. Dung, T. Hoang, T.D. Lam, T.V. Thu, D.T. Chien, P.N. Hong, P.N. Minh, N.V. Quynh, L.T. Lu, J. Electron. Mater. 49 (2020) 4671–4679. https://doi.org/10.1007/s11664-020-08165-z
13. D.T.T. Thủy, L.T.M. Hạnh, H.T. Dũng, D.T. Tùng, L.T. Lư, T.D. Lâm, N.T. Dung, J. Chem. 58 (5E1–2) (2020) 83–86.
14. V. V. Trong, N. T. T. Mai, D. T. Thuy, N. L. Huy, N. V. Anh, N. T. Dung, Electroanalysis, 34 (9) (2022), 1478-1486. https://doi.org/10.1002/elan.202100643
15. D.T. Tung, H.M. Nguyet, N.T. Dung, H.T. Dung, N.T. Yen, N.B. Thanh, P.N. Hong, P.V. Hoi, N.V. Quynh, P.N. Minh, L.T. Lu, J. Electron. Mater. 50 (2021) 4407–4414. https://doi.org/10.1007/s11664-021-08959-9
16. Z. Ming, C. Yan, Y. Dingyu, L. Jitao, J. Energy Storage 29 (2020) 101363. https://doi.org/10.1016/j.est.2020.101363
17. H.L. Nguyen, H.H. Cao, D.T. Nguyen, V.-A. Nguyen, Electroanalysis 29 (2017) 595–601. https://doi.org/10.1002/elan.201600438
18. M. Zhang, D. Yang, J. Li, J. Energy Storage 29 (2020) 101511. https://doi.org/10.1016/j.est.2020.101511